

# Global frequency selection in the observed time-mean wakes of circular cylinders

MOSES KHOR<sup>1</sup>, JOHN SHERIDAN<sup>1,2</sup>,  
MARK C. THOMPSON<sup>1,2</sup> AND KERRY HOURIGAN<sup>1,2</sup>

<sup>1</sup>Fluids Laboratory for Aeronautical and Industrial Research (FLAIR), Department of Mechanical and Aerospace Engineering, Monash University, Melbourne, Victoria 3800, Australia

<sup>2</sup>Division of Biological Engineering, Monash University, Melbourne, Victoria 3800, Australia

(Received 10 December 2006 and in revised form 1 February 2008)

Observations have been made of the time-mean velocity profile at midspan in the near-wake of circular cylinders at moderate Reynolds numbers between 600 and 4600, well beyond the Reynolds number of approximately 200 at which the wake becomes three-dimensional. The measured profiles are found to be represented quite accurately by a family of function profiles with known linear instability characteristics. The complex instability frequency is then determined as a function of wake position, using the function profiles. In general, the near wake undergoes a transition from convective to absolute instability; the distance downstream to the point of transition is found to increase over the Reynolds number range investigated. The emergence of a significant region of convective instability is consistent with the known appearance of Bloor–Gerrard vortices. The selected frequency of the wake instability is determined by the saddle-point criterion; the Strouhal numbers for Bénard–von Kármán vortex shedding are found to compare well with the values in the literature.

---

## 1. Introduction

The application of linear stability analysis has greatly advanced our understanding of shear flows. The analyses of time-mean velocity profiles focused initially on plane mixing layers, as characterized by the hyperbolic-tangent profile (Michalke 1964, 1965*a*, *b*). Subsequent application to the near wake of bluff bodies was undertaken. Early linear stability analyses, based on time-mean velocity profiles, concentrated on the fully developed wake far downstream of the body, such as those by Sato & Kuriki (1961) and Mattingly & Criminale (1972). Using inverted top-hat velocity profiles, Koch (1985) and Monkewitz & Nguyen (1987, hereafter referred to as MN) investigated the nature of the stability in the near wake. Betchov & Criminale (1966) and Mattingly & Criminale (1972) conjectured that the response of the flow to small perturbations is dominated by the resonance between a downstream- and an upstream-travelling instability wave. The amplification or damping of this resonance is related, respectively, to the absolute or convective character of the instability, as discussed by Briggs (1964).

Much of the earlier work on wake instability, as reviewed by Huerre & Monkewitz (1985), was stimulated by the studies of instabilities in plasmas by Briggs (1964) and Bers (1975). The concepts of absolute and convective instabilities were found useful in characterizing wakes and their response to perturbation. These characteristics are determined by the impulse response of a flow, which is defined as the instability-wave

field generated by a concentrated pulse in space and time. If an impulsively generated small-amplitude wave packet grows exponentially at the location of its generation, the flow is absolutely unstable. However, if that wave packet grows as it is convected downstream and leaves the flow at the location of its generation ultimately undisturbed, the flow is convectively unstable.

Betchov & Criminale (1966) and Koch (1985) conjectured that the Bénard–von Kármán vortex formation is an intrinsic response of wake flows arising from the absolute nature of the wake instability. The experiments of Provansal, Mathis & Boyer (1987) and Strykowski (1986) at Reynolds numbers near the onset of the Bénard–von Kármán vortex formation supported the idea that the vortex formation process is the result of self-excited oscillations of the wake. The self-excited nature is indicative of an absolute instability, which in turn explains the difficulty in suppressing the Bénard–von Kármán vortex formation by external excitation (Monkewitz 1974).

Furthermore, the investigation by Chomaz, Huerre & Redekopp (1988) with a Ginzburg–Landau model equation showed that a local absolute instability is a necessary though not a sufficient condition for a global mode to become self-excited. They found that the region of local absolute instability has to reach a finite critical size before the wake achieves self-excitation, the size of the region being dependent on a global control parameter such as the Reynolds number. Using a two-parameter family of functions to represent the time-mean velocity profiles of the cylinder wake, Monkewitz (1988) solved the Orr–Sommerfeld equation and deduced the absolute or convective nature of these profiles on a locally parallel basis as a function of the two parameters. These functions were then used to fit the measured time-mean velocity profiles from Nishioka (1973) and a numerical-simulation profile from Fornberg (1980) for various Reynolds numbers below and above the onset of the Bénard–von Kármán vortex formation. In this manner, it was shown that at the onset, a sufficiently large region of absolute instability had already formed in the near wake of the cylinder.

The calculations of Monkewitz (1988), however, could not yield a unique Bénard–von Kármán vortex frequency. This is because, as the mean flow develops spatially, a unique mode grows temporally in place at each downstream position within this substantial absolutely unstable region. An additional global mode selection criterion was therefore required to select the mode that corresponds to the observed global response. This issue is tackled in the analysis by Pierrehumbert (1984) in the context of atmospheric flows, and by Koch (1985) and MN in the context of inviscid, incompressible and locally parallel wake flows. Others have also made the connection between the global wake frequency and the absolute instability frequency curve derived from measured or model wake profiles (Betchov & Criminale 1966; Triantafyllou, Triantafyllou & Chryssostomidis 1986; Monkewitz 1988; Hannemann & Oertel 1989; Karniadakis & Triantafyllou 1989; Huerre & Monkewitz 1990; Huerre & Rossi 1998). A number of conjectures were made on the determination of the frequency of the global instability: Pierrehumbert (1984) proposed that the fastest growing resonance between the upstream and downstream instability waves dominates the absolutely unstable flow; Koch (1985) proposed that any downstream point where the local instability character changes from an absolute to a convective nature could act as a reflector for instability waves; MN introduced the initial resonance criterion (IRC), which states that the first local resonance with a non-negative absolute growth rate that the flow encounters will dominate the wake (see Pier *et al.* 1998 who first discussed the validity of the IRC as a fully nonlinear theory). The IRC is the bluff-body wake counterpart of the initial maximum growth rate criterion applied to convectively

unstable mixing layers (Ho & Huerre 1984). The inverted top-hat velocity profile represents the limit of the initial velocity profile from a bluff body, and so was used in the studies by Koch (1985) and MN. These criteria are however largely *ad hoc*.

More recently, a criterion for frequency selection has been established in a strictly linear setting (Chomaz, Huerre & Redekopp 1991; Monkewitz, Huerre & Chomaz 1993; Le Dizès *et al.* 1996). With this criterion, the complex global frequency is given by a saddle-point condition based on the analytic continuation of absolute instability frequency in the complex  $x = (x_r, x_i)$ -plane. In the case of the wake of a blunt-edged plate, Hammond & Redekopp (1997) obtained an accurate prediction of the frequency selected by the system based on the saddle-point theory applied on the time-mean flow. Consistent with this result, Pier (2002) found that the time average of the oscillating wake provided the best profile from which to predict the vortex shedding frequency for a similar configuration in the case of Reynolds number up to 200. Barkley (2006) has recently undertaken accurate two-dimensional (global) linear stability analyses of the mean flow of vortex shedding from a circular cylinder for Reynolds numbers between 46 and 180. His analysis found that the eigenfrequency of the time-mean flow tracked closely the Strouhal number of vortex shedding, consistent with the findings of Hammond & Redekopp (1997) and Pier (2002). Thiria & Wesfreid (2007) have similarly investigated the measured time-averaged flow as the base state to account for the stability properties of wakes under forcing conditions. Sipp & Lebedev (2007) have undertaken a global weakly nonlinear analysis valid in the vicinity of the first Hopf bifurcation at around  $Re = 47$ . They find that two conditions, involving parameters related to the nonlinear interactions in the wake, need to be satisfied: (a) for the time-mean flow to be approximately marginally stable, and (b) for the stability of the time-mean flow approximately to yield the nonlinear frequency of the limit cycle. The physical meaning of these two conditions is that the saturation process on the limit cycle is linked to the mean flow harmonic. The results of Sipp & Lebedev (2007) provide theoretical support to the numerical observations of Barkley (2006), and the current study which is extended to higher Reynolds numbers.

In contrast, linear stability analysis of the steady base flow provides eigenfrequencies that are quite different at these low Reynolds numbers and increasingly so as the Reynolds number is increased. However, use of the nonlinear stability criterion on steady base flows, determination of ‘elephant’ modes, and in some cases comparison with other stability criteria, have been presented by a number of researchers and shown to produce reasonable results (Chomaz 2003; Gallaire *et al.* 2006; Lesshafft *et al.* 2006; Marquillie & Ehrenstein 2003; Pier *et al.* 1998; Pier & Huerre 2001*a, b*; Pier, Huerre & Chomaz 2001; Pier 2002; Barkley 2006). It is interesting to note that Pier & Huerre (2001*a*) showed that the IRC criterion of MN is the one that selects these nonlinear ‘elephant’ modes.

In the present article, the analysis is focused on the time-mean flows and the use of local linear stability analysis and the saddle-point criterion to determine the global frequency selection in the wake of circular cylinders.

### 1.1. *The scope of the present study*

The unanswered questions that arise from the previous studies are:

1. Is the saddle-point criterion capable of determining the global instability frequency for observed time-mean cylinder wakes at Reynolds numbers beyond the previously examined limit of 200, where the time-dependent wakes become three-dimensional?

2. How applicable are the MN  $1/N$  profiles in the determination of wake stability characteristics, and can they be used to avoid the necessity of solving the Rayleigh equations?

3. How does the point of transition from convective to absolute instability vary with Reynolds number?

4. Does the emergence of a significant region of convective instability align with the appearance of Bloor–Gerrard vortices (Bloor 1964) as reported in the literature?

To address the above questions, detailed observations of the time-mean velocity profiles in the near wake of a circular cylinder were made. The measurements were taken using a hot wire mounted on a traversing mechanism with high spatial resolution. The measured profiles were fitted with the two-parameter family of functions, the instability characteristics of which had been determined in the study by MN. The evolution of the character of the near-wake instability, in particular the applicability of the saddle-point criterion for mode selection, was then studied. The presence of a convectively unstable region in the near wake of a circular cylinder, proposed by MN, was also examined.

The current work extends the analyses using computational fluid dynamics predictions of the time-mean flow of Pier (2002) and Barkley (2006) from lower Reynolds numbers, at which the time-dependent flow is two-dimensional, to the analysis of experimentally observed wakes of flows around circular cylinders at moderately high Reynolds numbers, where the flow is three-dimensional.

## 2. Experimental methods

A brief description of the wind tunnel, instrumentation, and data acquisition is given below.

### 2.1. Wind tunnel

The open-circuit wind tunnel had a working section a  $244 \times 244$  mm cross-section and a very low free-stream turbulence level: 0.07% of free-stream velocity at the tunnel flow speed of  $3.3 \text{ m s}^{-1}$ . The hot-wire signal was band-pass filtered between 20 and 1400 Hz. The flow was also highly uniform with a coefficient of variation across the whole cross-section of 0.0027. The flow velocity in the working section could be varied continuously from 1 to  $35 \text{ m s}^{-1}$ .

### 2.2. Instruments

Velocity measurements were taken with a TSI IFA-100 constant-temperature anemometer, and a TSI 1210-T1.5 hot-wire probe (the diameter of the wire was  $4 \mu\text{m}$ ). The signal was processed through a Rockland 852 band-pass filter, and acquired with a Boston Technology PC-30DS 12-bit ADC card mounted on an IBM PC. A Pitot-static tube connected to a Van Essen 11934 Betz micro-manometer was used to take initial velocity measurements. The uncertainty in the velocity measured thus was approximately 4%. These measurements were used to calibrate the hot-wire anemometry system in the wind tunnel. The uncertainty associated with the hot-wire anemometer was approximately 6%.

An X-Y motorised linear traversing mechanism was constructed to traverse a hot wire across the near wake of a circular cylinder, the hot wire being aligned parallel to the cylinder axis. The mounting-stage was connected to a THK MTF-0601 ball-screw mechanism and controlled by a Superior Electric Slo-Syn stepping motor which stepped through 200 steps/revolution. Each step of the traverser corresponded to a movement of  $5 \mu\text{m}$  to within  $\pm 0.13$  microns.

The three polished Perspex cylinders used in the investigation were 244 mm long with diameters  $D$  of 6.29, 9.44 and 12.6 mm resulting in blockages of 2.6 %, 3.9% and 5.2 %, respectively. Circular end-plates were mounted to reduce the influence of the boundary layer of the wind tunnel. Consequently, the effective aspect ratios of the cylinders were 32.1, 21.4 and 16.0, respectively. The coordinate system origin was at the centre of the cylinders midway along their length. The  $x$ -axis was in the direction of the flow, the  $y$ -axis was perpendicular to the flow, and the  $z$ -axis coincided with the cylinder axis.

### 2.3. Data acquisition

The experimental program covered the  $Re$  range of between 600 and 4600. Depending on the size of the cylinder used, the spacing between each  $y$ -station ranged between 35 and 75  $\mu\text{m}$ . The number of  $y$ -stations was sufficient to measure the time-mean velocity profile. Owing to the symmetry of the time-mean velocity profile of circular cylinder wakes, only half the wake was traversed. Depending on the size of the cylinder used, the spacing between each  $x$ -station ranged between 1 and 2 mm. This resulted in the velocity profile being mapped from directly above the cylinder ( $x/D=0$ ) to a distance downstream of  $x/D=1.03$ . The experiments were originally conducted under the assumption that the initial resonance criterion could provide the governing frequency. The point at which the flow shows transition from convective to absolute instability (i.e. where the initial resonance criterion would have been applied) was found in nearly all the cases studied to occur in the domain  $0 < x/D < 1$ . Subsequently, it was learned that the saddle-point criterion was the appropriate stability criterion for time-mean flows. Fortunately, the real component of the saddle point was found to be located near  $x/D$  unity, lying within the measurement domain or requiring only minor extrapolation.

For low Reynolds numbers (of order  $10^2$ ), the wake of shorter finite circular cylinders can exhibit separate vortex shedding, at different frequencies, near the cylinder ends and in the mid-region (Gerich & Ecklemann 1982). As the Reynolds number is increased, the vortex shedding becomes coupled along the span at a frequency between the previous separate frequencies. At higher Reynolds number, the typical time-mean near wake behind the circular cylinder becomes uniform along much of the span, with end effects confined to close to the walls or endplates (e.g. as shown by the base pressure coefficient along the span of the cylinder in by Bearman 1969). Similar to Norberg (1987), the measurements in the current experiments were taken in the near wake at the midspan of the cylinder.

At each sampling station, the hot-wire signal was sampled at 1500 Hz (which was found to be sufficient for all frequencies of interest), and the sample length was 16 384. The data were then processed to calculate the mean and fluctuating velocities at each sampling station. In addition, the data were also spectrally analysed to ensure that the signals were not contaminated by signal noise.

### 2.4. The function velocity profile and fitting the measured profiles

Linearization of the equations governing the flow and neglecting viscous effects results in the Rayleigh equation, the boundary condition of which can be set to force the solution to be either purely symmetric (varicose mode) or antisymmetric (sinuous mode). In the present study, only the sinuous mode was investigated as we are concerned with the instability resulting in the Bénard–von Kármán shedding.

In principle, the Rayleigh equation could be solved for each velocity profile. However, the velocity profile data available for this study did not extend to the centreline axis of the wake owing to limitations of the hot wire at low velocities. It

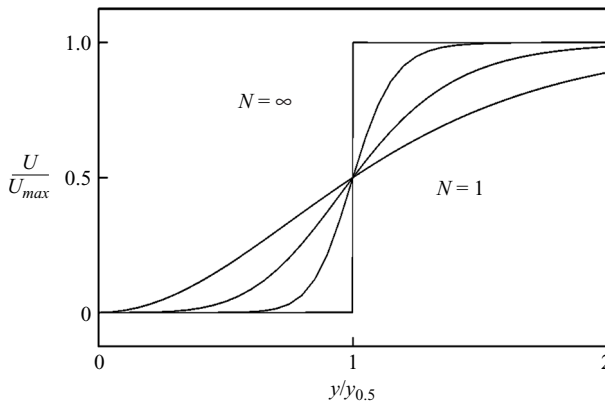


FIGURE 1. The dimensionless near-wake velocity profile defined by (2.1), with  $R = -1$ , for  $N = 1, 2, 5$ , and  $\infty$ .

was decided to employ the function velocity profiles used in the study of MN, for which the Rayleigh equation solutions have already been obtained, to fit the available data. It will be seen that the function profile fits are quite satisfactory and allow the determination of global frequency selection.

The function velocity profiles,  $u(y)$ , used by MN were of the form

$$u(y)/u_{max} = 1 - R + \frac{2R}{1 + \sinh^{2N}((y/y_{0.5}) \sinh^{-1} 1)}, \tag{2.1}$$

where  $y$  is the cross-stream coordinate,  $u_{max}$  is the maximum time-mean velocity in the profile, the half-wake width,  $y_{0.5}$ , is the position where  $u = u_{max}/2$ ,  $N$  is the shape parameter, and  $R$  is the velocity ratio:

$$R = \frac{u(y = 0) - u(y \rightarrow \infty)}{u(y = 0) + u(y \rightarrow \infty)}, \tag{2.2}$$

which allows the depth of the wake to be adjusted. Values of  $R > 0$  correspond to jet profiles, while  $R = -1$  corresponds to a wake with zero centreline velocity. As stated by MN: “in a typical bluff-body wake these parameters will be functions of  $x$ , starting at some large  $N$  and  $R \rightarrow -1$  right behind the body, and approaching  $N = 1$  and  $R = 0$  for large  $x$ ”. Therefore, the parameter  $N$  allows the profile to be continuously changed from a top-hat wake bounded by two vortex sheets, when  $N = \infty$ , to the far-wake  $\text{sech}^2(y)$  profile, when  $N = 1$ . Figure 1 illustrates the variation of half the wake with  $N$ . It is important to note that the half-wake profile is in general asymmetrical about  $y_{0.5}$ . However, the half-wake tends towards symmetry about  $y_{0.5} = 1$  as  $N \rightarrow \infty$ , and is approximately so even for moderate values of  $N$ .

As in MN, the analysis will proceed with the assumption that the transition to absolute instability occurs for wakes for which the recirculation velocity is small; that is,  $R = -1$ . A small backflow will, according to the analysis of MN, change the local absolute instability frequency by a similarly small amount. Although we find that the MN profiles can fit well the velocity profiles in the rapidly varying region across the shear layer, it is not clear that they would be able to handle simultaneously any non-zero velocities along the centreline. It is noted that MN studied the effect of backflow by keeping  $R = -1$  and introducing another parameter to mimic backflow. Although the fitting of the MN curves was therefore terminated at the half-width, the predicted Strouhal numbers are found to appear remarkably

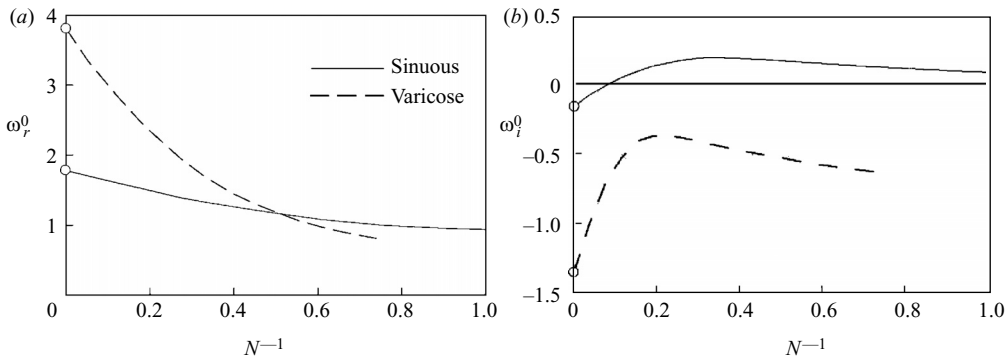


FIGURE 2. The (a) real and (b) imaginary parts of the branch point frequency of the dispersion relation for the velocity profile (2.1) with  $R = -1$ , as a function of  $N^{-1}$ . After MN.

consistent with the literature. Future studies are planned to use computational and non-invasive experimental techniques being developed to provide full and low-scatter velocity profiles for which the Rayleigh equation can be solved.

Figure 2, based on MN, shows the real and imaginary parts of the absolute instability frequency,  $\omega^0$ , of the dispersion relation for the velocity profile (2.1) with  $R = -1$ , as a function of the shape parameter  $N$ . The figure shows the positive absolute growth rate  $\omega_i^0 > 0$ , which indicates absolute instability, for  $1/N > 0.08$ . The corresponding real component of the absolute instability frequency is  $\omega_r^0 = 1.68$ .

As mentioned above, the value of  $R$  was chosen to be  $-1$ , because in the near wake of a circular cylinder the flow is approximately stagnant (it is the low flow velocities in this region that render the hot-wire technique inappropriate). The value of  $N$  to fit the experimental profile was chosen to minimize the perpendicular distance between the measured time-mean velocity data point and the function velocity profile (the RMS of this perpendicular distance was typically less than 0.1% of the mean height. Two other methods of optimization, incorporating also velocity, were tested but the selected method performed best). Typical fits are provided in the results section below.

### 2.5. Frequency

The complex absolute Strouhal number,  $St = (St_r, St_i) \equiv (\omega_r^0, \omega_i^0)/(4\pi y_{0.5}/D)$ , at the complex saddle point,  $x_s \equiv (x_{sr}, x_{si})$ , for each Reynolds number was determined using the following procedure.

(a) The transverse mean velocity profiles through the separating shear layer were obtained at successive  $x_r$ -stations along the wake.

(b) The real and imaginary components of the Strouhal number at each  $x_r$ -station were obtained by fitting the data using the functional form suggested by MN. This was achieved by varying the fitting parameter  $N$  to minimize the sum of (absolute) differences between the fit and data points. Once  $N$  was found, the real and imaginary components of the frequency were obtained from a lookup table derived from figure 2.

(c) At this stage the real and imaginary components of the Strouhal number as a function of downstream distance  $x_r$ , i.e. along the real axis, are known. Generally, the maximum growth rate (the imaginary component of complex frequency) and the frequency (the real component), do not coincide. This is an indication that the saddle point,  $x_s$ , lies off the real axis in the complex plane. To extrapolate off the real axis, the following procedure is used (Huerre & Monkewitz 1985).

(d) Using the information on the real axis, the behaviour of the complex frequency off-axis can be extrapolated using Taylor series assuming the function remains analytic. The expressions for the real and imaginary components of the Strouhal number are

$$St_r(x) = St_r(x_r, x_i = 0) + \left. \frac{\partial St_r}{\partial x_i} \right|_{x_i=0} x_i + O(x_i^2) = St_r(x_r, x_i = 0) - \left. \frac{\partial St_i}{\partial x_r} \right|_{x_r=0} x_i + O(x_i^2), \quad (2.3)$$

$$St_i(x) = St_i(x_r, x_i = 0) + \left. \frac{\partial St_i}{\partial x_i} \right|_{x_i=0} x_i + O(x_i^2) = St_i(x_r, x_i = 0) + \left. \frac{\partial St_r}{\partial x_r} \right|_{x_r=0} x_i + O(x_i^2). \quad (2.4)$$

Here, the final expression in each equation has been obtained by replacing the derivatives with respect to  $x_i$  with derivatives with respect to  $x_r$  using the Cauchy–Riemann equations.

(e) Quadratic functional approximations to  $St_r$  and  $St_i$  on the real axis are derived using data from the stability analysis. These approximations can be used to estimate the Strouhal number and derivative terms on the right-hand sides of equations (2.3) and (2.4) (Hammond & Redekopp 1997), so that the Strouhal number components about the saddle point are expressed in terms of  $x_r$  and  $x_i$ .

(f) Finally, because  $x_s$  is a saddle point so that

$$\left. \frac{\partial St}{\partial x} \right|_{x=x_s} = 0, \quad (2.5)$$

then by taking the derivative of equations (2.3) and (2.4) and equating to zero, allows  $x_s \equiv (x_{sr}, x_{si})$  to be determined, which in turn allows  $St = (St_r, St_i)$  to be determined.

### 3. Results and discussion

#### 3.1. Observed wakes: Reynolds number 600 to 4600

In this section, the stability analysis to determine the global frequency selection is applied to the detailed time-mean velocity and velocity fluctuation data of Khor (1998) in the near wake of circular cylinders for Reynolds number from 600 to 4600.

##### 3.1.1. Fluctuating velocities and time-mean velocity profiles

The growth of the maximum fluctuating velocity in the near wake of the circular cylinder is shown in figure 3. The maximum fluctuating velocity,  $u'_{max}$ , was chosen because it was a reliable and repeatable measurement that could be unambiguously distinguished from among the fluctuating velocity data across the shear layer, at all streamwise stations. Comparison between the present measurements of  $u'_{max}$  with the measurements of  $u'_{edge}$  by Unal & Rockwell (1988) show that the two quantities display the same characteristic exponential growth in the streamwise direction.

Figure 3 shows that the growth of the fluctuating velocity peaks at around  $x/D = 1.5 - 2.0$ . If the streamwise ( $x/D$ ) position where  $u'_{max}$  peaks for each  $Re$  approximates the formation length of the Bénard–von Kármán vortices, then the complete set of measurements for all the Reynolds numbers studied showed that the formation length increased between  $Re$  of 600 and roughly 2000, and decreased

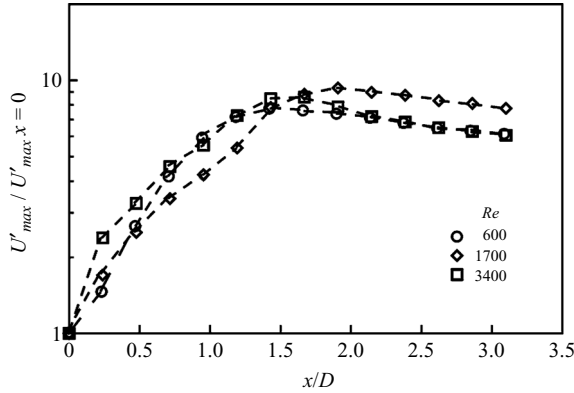


FIGURE 3. The growth of  $u'_{max}$ , normalized by the  $x/D=0$  data point and plotted on a log-linear graph, in the wake of the circular cylinder.

between  $Re = 2000$  and  $5000$ . This increase and decrease in the formation length is in agreement with the flow visualizations of Unal & Rockwell (1988).

Examples of the curve-fitting procedure are shown in figure 4 for  $Re = 600$  and  $Re = 1700$ . The filled circles are the data points used for the curve-fitting. Data points for which  $u/u_{max} < 0.5$  were not used because hot-wire measurements at low flow speeds become less accurate owing to the free convection from the hot wire. Data points from cross-stream stations further out from the station where  $u/u_{max} = 1$  were also discarded in order that there was a uniform cutoff point for every streamwise station, for every experimental run. A sensitivity analysis was carried out to evaluate the effect of varying the lower cutoff point from  $u/u_{max} = 0.5$  down to  $u/u_{max} = 0.25$ . It was found that the values of  $N$  selected varied little.

The half-wake width,  $y_{0.5}$ , is the coordinate where  $u(y) = 0.5u_{max}$ ; its position effectively tracks the shear layer. The half-wake width data for all the streamwise stations for different  $Re$  were determined and are presented in figure 5. The half-wake width data across the  $Re$  range are seen to spread over approximately  $0.2D$ .

### 3.1.2. Transition to absolute instability and global frequency selection

At each station along the axis where the velocity profile was measured, the real and complex components of the absolute Strouhal number,  $St_r$  and  $St_i$ , respectively, associated with the local absolute instability frequency are plotted in figure 6 for each Reynolds number. All of the curves show a global minimum in the real component  $St_r$  and a global maximum in the imaginary component  $St_i$  in the vicinity of  $x/D$  being unity. For each Reynolds number, a least-squares quadratic fit was performed from which the frequencies and derivatives were obtained.

Figure 7 shows the location,  $x_{ca}$ , along the wake at which the flow first becomes locally absolutely unstable (i.e.  $St_i = 0$ ) and the real value of the saddle point,  $x_{rs}$ , as Reynolds number is increased. (The imaginary component of the saddle-point position,  $x_i$ , was generally found to be close to zero, consistent with the expansions used in equations (2.3) and (2.4)). The transition to absolute instability in the wake generally moves downstream as the Reynolds number increases. The real component of the saddle point generally lies beyond the point of transition to absolute instability, as would be expected. Curiously, for the higher Reynolds numbers, the results were not so clear cut; in the case of  $Re = 4035$ , no positive  $St_i$  were recorded and for  $Re = 4600$ , the trend lines appear to be converging.

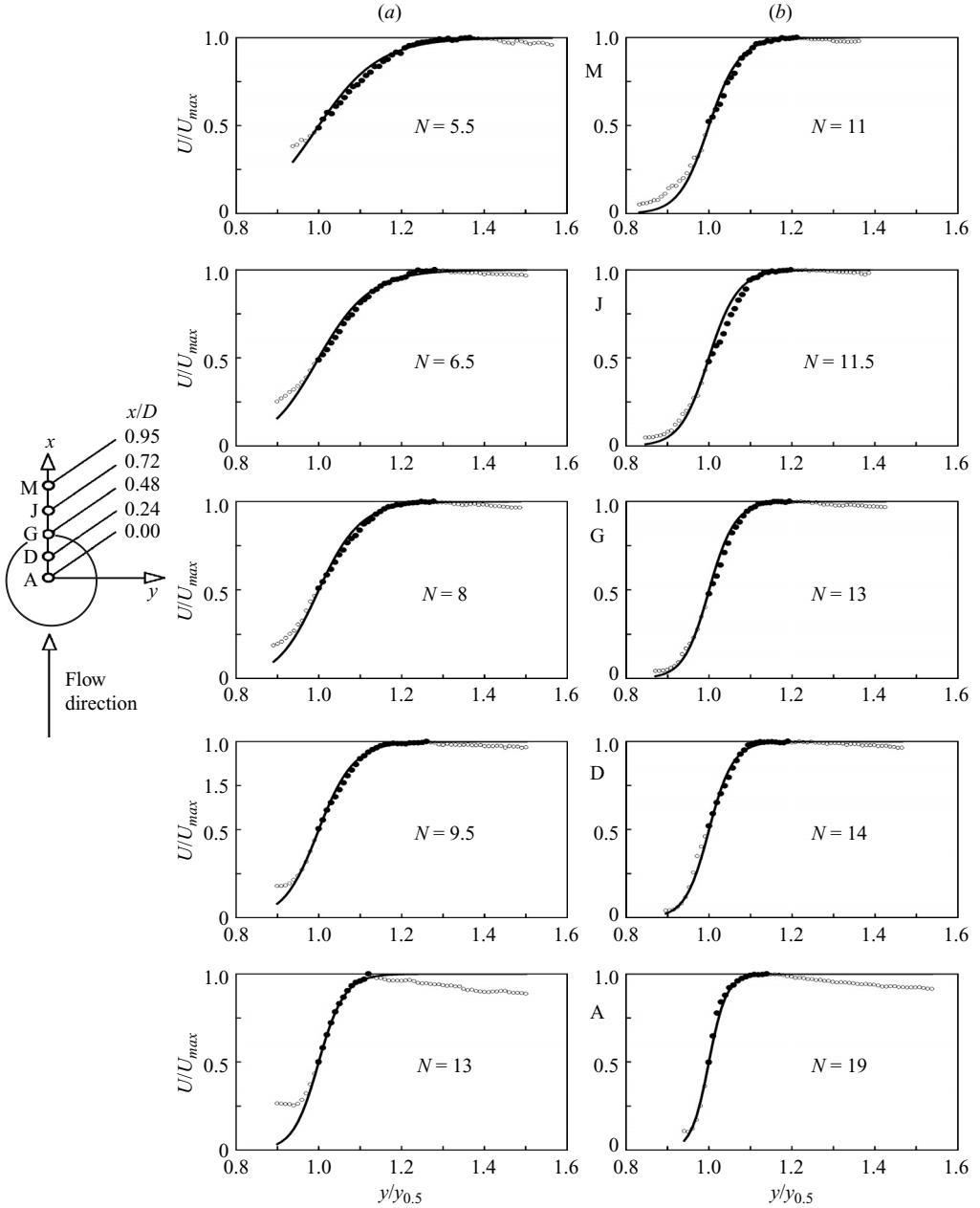


FIGURE 4. Time-mean velocity profiles of the wake of the circular cylinder for  $Re = 600$ ;  $D = 6.29$  mm (a) and  $Re = 1700$ ;  $D = 9.44$  mm (b). The filled circles are the data points used for fitting with the function velocity profiles, shown as solid lines. The values of  $N$  were chosen to minimize the perpendicular distance between experimental data and function.

The development of Bloor–Gerrard instability waves to significant levels in the separating shear layer requires both a significant region of convective instability and a distance of about two wavelengths of shear layer to allow significant growth (Freymuth 1966). As the Reynolds number increases above  $Re \approx 10^3$ , a significant portion (of the order of the wavelength of the instability according to the frequency

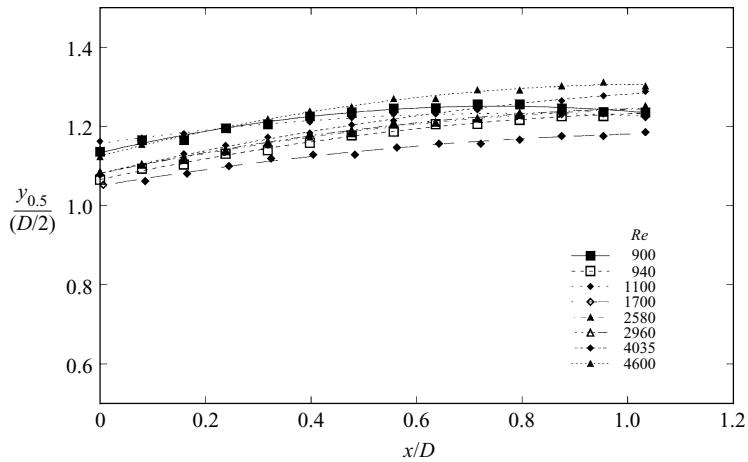


FIGURE 5. Variation of the non-dimensionalized wake half-width,  $y_{0.5}$ , with streamwise distance,  $x/D$  for a selection of Reynolds numbers.

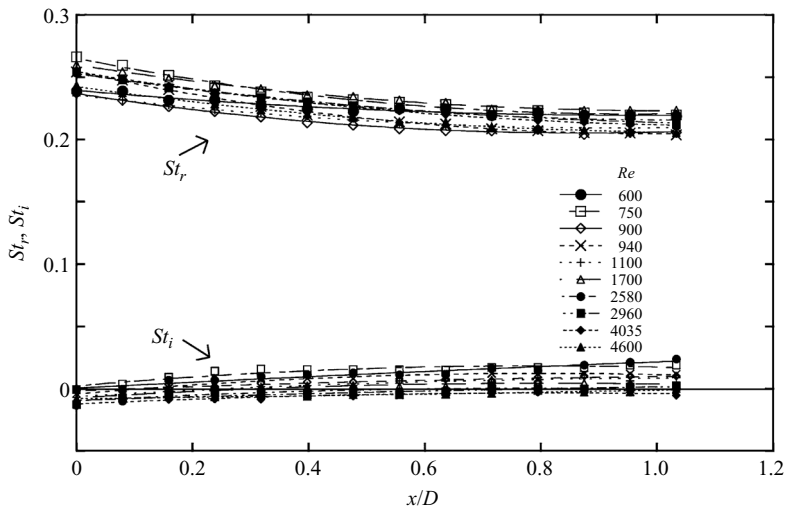


FIGURE 6. The real and imaginary components,  $St_r$  and  $St_i$ , of the absolute Strouhal number obtained from the MN functions along the wake for a range of Reynolds numbers. Least-squares quadratic fits are shown.

fit of Prasad & Williamson 1997) of the near wake becomes convectively unstable, whereas for  $Re < 10^3$ , the near wake is only marginally convectively unstable. The distance to the formation region at  $Re \approx 10^3$ , again using the frequency fit of Prasad & Williamson (1997), also exceeds twice the instability wavelength. The emergence in the wake of a significant region of convective instability sufficient to support the development of the higher frequency Bloor–Gerrard instability waves, and with sufficient distance to grow, is consistent with a range of general low-turbulence studies that found that this convective instability first appears naturally in the separating shear layers at Reynolds numbers greater than  $10^3$  or higher (Bloor 1964; Kourta *et al.* 1987; Norberg 1987; Wei & Smith 1986; Prasad & Williamson 1997; Unal & Rockwell 1988). The presence of the convectively unstable region in the near wake, as

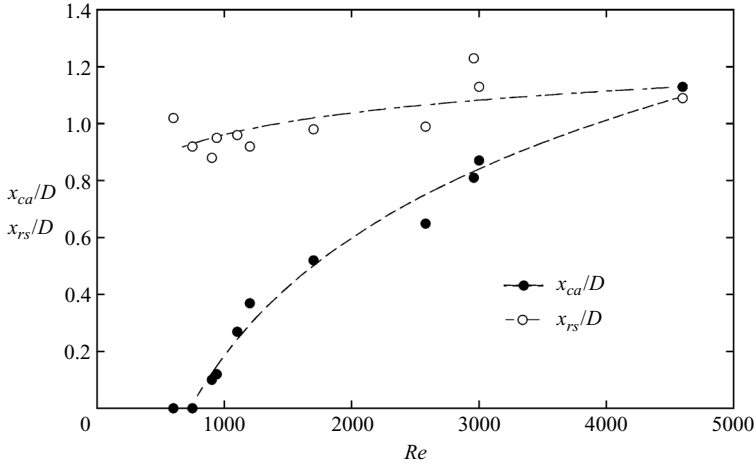


FIGURE 7. Distance  $x_{ca}$  downstream in wake to appearance of absolute instability region and real component of the saddle point position,  $x_{rs}$ , for different Reynolds numbers  $Re$ .

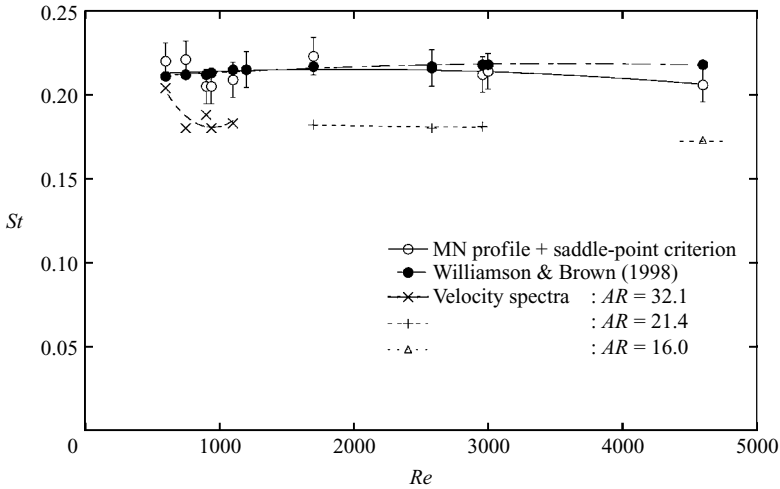


FIGURE 8. Comparison of the predicted Strouhal numbers based on the MN fits and saddle-point criterion (5% error bars shown) with the curve fit of Williamson & Brown (1998). The lower Strouhal numbers determined from the velocity spectra are also shown together with the associated cylinder aspect ratio,  $AR$ .

found in this study, also confirms the finding of MN who came to the same conclusion by calculating the  $N$  values from the measured wake vorticity thickness.

Figure 8 shows the absolute Strouhal numbers obtained using the saddle-point criterion and those determined from the power spectra of the velocity time series. Also shown are the Strouhal numbers from the fit of Williamson & Brown (1998). The spectral peaks associated with the vortex shedding were found to be consistent from the hot-wire measurements at various locations both across the shear layers and different stations along the wake. It is noted that the  $St$  observed from the velocity spectra in this study tend to be about 10% lower than those reported in the literature, consistent with the effect of the lower cylinder aspect ratios, as shown by Norberg (1994).

One trend that emerges (see figure 8) is that although the absolute Strouhal numbers calculated using stability theory tend to be in general greater than the observed values, they match reasonably well (within 5%) the values of 0.20 – 0.22 obtained for higher aspect ratio cylinders with end effects carefully controlled (e.g. Norberg 1994; Williamson & Brown 1998; Williamson 1989). The stability studies using the saddle-point criterion are based on the velocity profiles at the midspan of the cylinders and in the near wake, and therefore are expected to be relatively unaffected by the end conditions, producing Strouhal number predictions consistent with observed values for large-aspect-ratio cylinders.

### 3.1.3. *Validity and accuracy of global frequency selection*

Approximations and errors arise in the preceding analyses through a variety of sources and it is important to acknowledge these. The use of the MN profiles and their related stability characteristics assumes that the flows are nearly parallel in the regions where the stability study is undertaken. Hammond & Redekopp (1997) examined the parallel assumption for vortex shedding from interacting boundary layers at a blunt trailing edge. They found that their measure of the non-parallelness of the wake ( $\epsilon$ ) peaked at about 25% downstream of the trailing edge. Close to the spatial position of the saddle point, the value was closer to  $\epsilon = 10 - 15\%$ . Despite this, the wake frequency from the saddle-point criterion based on the time-mean flow was within 1% of the observed wake frequency from direct simulations. For a circular cylinder, the non-parallelness is presumably slightly higher because of the non-equilibrium separating boundary layer, and because the separating streamline is not initially parallel to the wake centreplane. Nevertheless, the saddle-point frequency predictions, again based on the mean flow, are still within a couple of percent between  $Re = 100 - 200$  (Pier 2002). To close the loop, Barkley (2006) numerically and Sipp & Lebedev (2007) theoretically showed that a global frequency analysis based on the time-mean flow accurately predicts the observed shedding frequency in this Reynolds number range. Thus the global stability analysis and the saddle-point criterion applied to the local analysis assuming near-parallel flow provide predictions for the circular cylinder wake within a few percent of each other for the two-dimensional low Reynolds number flow regime. After the transition to three-dimensionality at  $Re \simeq 190$  (Barkley & Henderson 1996), the separation point (indicated by the angle,  $\theta$ , from the midpoint on the rear surface) moves from before the top of the cylinder ( $\theta = 95^\circ$ ) at  $Re = 300$  to  $\theta = 91^\circ$  at  $Re = 1500$  and  $\theta = 82^\circ$  at  $Re = 12000$  (Zdravkovich 1997; Dimopoulos & Hanratty 1968), while the mean separation zone initially increases in length until it begins to shorten again at  $Re \simeq 2000$  when the shear-layer instability begins to have an effect (e.g. Prasad & Williamson 1997; Thompson & Hourigan 2005). Thus, it could be expected that the mean wake is more parallel in the Reynolds number range considered in this paper than in the two-dimensional shedding regime.

In addition to the assumption of near-parallel flow, the stability analysis associated with the MN profiles also assumes that the effect of viscosity is negligible. Hammond & Redekopp (1997) explicitly compare saddle-point frequency predictions from an Orr–Sommerfeld and a Rayleigh solver at a low Reynolds number of  $Re = 160$  for their interacting boundary layer wake. They find only a 2% difference in the frequency predictions. It is expected that for the higher Reynolds numbers considered here, the inviscid assumption is valid. As shown by Norberg (1987), changes to the Strouhal number and the vortex formation length can arise owing to the effect of cylinder aspect ratio (end effects). Decreasing the aspect ratio was found to reduce the observed Strouhal number, typically of the order 10% for the spans

used in the present experiments. The stability analysis in the present work is based only on the velocity profile taken at the midspan of the cylinder; the global frequencies calculated on this basis are generally higher than those manifested physically, but consistently match reasonably well those for very large spans according to Williamson & Brown (1998).

The use of hot wires is an effective means of obtaining time-mean velocity profiles, and the existing data have allowed a comprehensive stability study to be undertaken; however, hot wires do represent a physical intrusion to the flow. In the future, it is planned to obtain more detailed full wake data, including the low-velocity near-axis recirculation zone, through the application of non-intrusive flow measurement techniques, such as particle image velocimetry. These should provide more detailed instantaneous flow velocity fields as well as time-mean fields as new methods are being developed (e.g. Fouras, Distingu & Hourigan 2007a; Fouras *et al.* 2007b; Fouras, Jacono & Hourigan 2008). Together with the ability of computational fluid dynamics to handle flows of increasing Reynolds number and the ability to track time-dependent perturbation fields (Thompson, Hourigan & Sheridan 1996; Leontini, Thompson & Hourigan 2007), further insights into the stability characteristics of the wake of the circular cylinder and other bluff body flows are expected.

#### 4. Conclusions

The present study has extended the stability study using the saddle-point criterion for circular cylinder flows into the three-dimensional shedding regime based on experimental observations; previous such studies have been undertaken for numerical predictions of two-dimensional flows at Reynolds numbers not greater than 200.

For the near wake of circular cylinders at Reynolds numbers between 600 and 4600, the absolute or convective nature of the instability has been examined by experimental and accompanying analytical methods.

In the Reynolds number range 600 – 4600, the time-mean velocity profiles with the function profiles of MN were measured. By adjusting the shape parameter,  $N$ , the function profiles could be fitted to the measured profiles as they varied downstream. MN had already calculated the absolute or convective instability character of these function profiles as a function of  $N$ . Therefore, the instability character of the developing wake was determined from the value of  $N$  used to fit the measured profiles, a process eliminating the need for separate linear stability solvers to be used. Another reason to employ a global fit is that the data have some associated noise, which means that it is difficult to use the data directly in a Rayleigh solver—especially as accurate second derivatives are required. The cylinders, with end-plates, employed in the present study were of aspect ratios between 16 and 32; consequently, their wakes had Strouhal numbers, based on the direct measurement of the vortex shedding frequencies, somewhat lower (typically 10 %) than those found for cylinders with large aspect ratios, in line with the observations of Norberg (1994). The Strouhal numbers obtained from the current stability analysis, using the velocity profiles at midspan, were in reasonable agreement with the values from the literature.

The results also showed the general presence of a zone of convective instability immediately downstream of the separation point of the shear layers. The flow undergoes transition to absolute instability further downstream as the wake develops and the separated shear layer thickens. The convectively unstable zone consequently grows in streamwise extent as  $Re$  increases, indicating that the transition point from convective to absolute instability moves downstream as  $Re$  increases. The development

of a significant convectively unstable region downstream only for Reynolds numbers beyond approximately 1000 is consistent with the initial appearance recorded in the literature of Bloor–Gerrard vortices in the shear layers.

We are greatly indebted to Martin Welsh for providing the experimental facilities at the CSIRO. Moses Khor acknowledges the support of a Monash Graduate Scholarship. We are grateful for support from Australian Research Council Large grant A89131241. The comments of the anonymous referees provided many improvements to the article.

## REFERENCES

- BARKLEY, D. 2006 Linear analysis of the cylinder wake mean flow. *Europhys. Lett.* **75**, 750–756.
- BARKLEY, D. & HENDERSON, R. D. 1996 Three-dimensional Floquet stability analysis of the wake of a circular cylinder. *J. Fluid Mech.* **322**, 215–241.
- BEARMAN, P. W. 1969 On vortex shedding from a circular cylinder in the critical Reynolds number regime. *J. Fluid Mech.* **37**, 577–585.
- BERS, A. 1975 Linear waves and instabilities. In *Physique des Plasmas* (ed. C. DeWitt & J. Peyraud), pp. 117–213. Springer.
- BETCHOV, R. & CRIMINALE, W. 1966 Spatial instability of the inviscid jet and wake. *Phys. Fluids* **9**, 359–362.
- BLOOR, M. 1964 The transition to turbulence in the wake of a circular cylinder. *J. Fluid Mech.* **19**, 290–304.
- BIGGS, R. J. 1964 *Electron-Stream Interaction with Plasmas*. MIT Press.
- CHOMAZ, J. M. 2003 Fully nonlinear dynamics of parallel wakes. *J. Fluid Mech.* **495**, 57–75.
- CHOMAZ, J. M., HUERRE, P. & REDEKOPP, L. 1988 Bifurcations to local and global modes in spatially developing flows. *Phys. Rev. Lett.* **60**, 25–28.
- CHOMAZ, J. M., HUERRE, P. & REDEKOPP, L. 1991 A frequency selection criterion in spatially developing flows. *Stud. Appl. Maths* **84**, 119–144.
- DIMOPOULOS, H. & HANRATTY, T. 1968 Velocity gradients at the wall for flow around a cylinder for Reynolds numbers between 60 and 360. *J. Fluid Mech.* **33**, 303–319.
- FORNBERG, B. 1980 A numerical study of steady viscous flow past a circular cylinder. *J. Fluid Mech.* **98**, 819–855.
- FOURAS, A., DUSTING, J. & HOURIGAN, K. 2007a A simple calibration technique for Stereoscopic Particle Image Velocimetry. *Exps. Fluids* **42**, 799–810.
- FOURAS, A., JACONO, D. L. & HOURIGAN, K. 2008 Target-free Stereo PIV: a novel technique with inherent error estimation and improved accuracy. *Exps. Fluids* **44**, 317–329.
- FOURAS, A., JACONO, D. L., SHEARD, G. J. & HOURIGAN, K. 2007b Measurement of instantaneous velocity and surface topography of a cylinder at low Reynolds number. In *Proc. IUTAM Symp. on Unsteady Separated Flows and Their Control* (ed. E. M. Braza & K. Hourigan), Corfu, Greece, 18–22 June.
- FREYMUTH, P. 1966 On transition in a separated laminar boundary layer. *J. Fluid Mech.* **25**, 683–704.
- GALLAIRE, F., RUTH, M., MEIBURG, E., CHOMAZ, J. M. & HUERRE, P. 2006 Spiral vortex breakdown as a global mode. *J. Fluid Mech.* **549**, 71–80.
- GERICH, D. & ECKLEMANN, H. 1982 Influence of end plates and free ends on the shedding frequency of circular cylinders. *J. Fluid Mech.* **122**, 109–121.
- HAMMOND, D. & REDEKOPP, L. 1997 Global dynamics of symmetric and asymmetric wakes. *J. Fluid Mech.* **331**, 231–260.
- HANNEMANN, K. & OERTEL, H. 1989 Numerical simulation of the absolutely and convectively unstable wake. *J. Fluid Mech.* **199**, 55–88.
- HO, C. M. & HUERRE, P. 1984 Perturbed free shear layers. *Annu. Rev. Fluid Mech.* **16**, 365–424.
- HUERRE, P. & MONKEWITZ, P. A. 1985 Absolute and convective instabilities in free shear layers. *J. Fluid Mech.* **159**, 151–168.
- HUERRE, P. & MONKEWITZ, P. A. 1990 Local and global instabilities in spatially developing flows. *Annu. Rev. Fluid Mech.* **22**, 473–537.

- HUERRE, P. & ROSSI, M. 1998 Hydrodynamic instabilities in open flows. In *Hydrodynamics and Nonlinear Instabilities* (ed. C. Godrèche & P. Manneville), pp. 81–294. Cambridge University Press.
- KARNIADAKIS, G. E. & TRIANTAFYLLOU, G. S. 1989 Frequency selection and asymptotic states in laminar wakes. *J. Fluid Mech.* **199**, 441–469.
- KHOR, M. 1998 The character of the near-wake instability of the circular cylinder. PhD thesis, Department of Mechanical Engineering, Monash University.
- KOCH, W. 1985 Local instability characteristics and frequency determination of self-excited wake flows. *J. Sound Vib.* **99**, 53–83.
- KOURTA, A., BOISSON, H., CHASSAING, P. & HA MINH, H. 1987 Nonlinear interaction and the transition to turbulence in the wake of a circular cylinder. *J. Fluid Mech.* **181**, 141.
- LE DIZÈS, S., HUERRE, P., CHOMAZ, J.-M. & MONKEWITZ, P. 1996 Linear global modes in spatially developing media. *Phil. Trans. R. Soc. Lond. A* **354**, 168–212.
- LEONTINI, J., THOMPSON, M. C. & HOURIGAN, K. 2007 Three-dimensional transition in the wake of a transversely oscillating cylinder. *J. Fluid Mech.* **577**, 79–104.
- LESSHAFFT, L., HUERRE, P., SAGAUT, P. & TERRACOL, M. 2006 Nonlinear global modes in hot jets. *J. Fluid Mech.* **554**, 393–409.
- MARQUILLIE, M. & EHRENSTEIN, U. 2003 On the onset of nonlinear oscillations in a separating boundary-layer flow. *J. Fluid Mech.* **490**, 169–188.
- MATTINGLY, G. E. & CRIMINALE, W. 1972 The stability of an incompressible two-dimensional wake. *J. Fluid Mech.* **51**, 233–272.
- MICHALKE, A. 1964 On the inviscid instability of the hyperbolic tangent velocity profile. *J. Fluid Mech.* **19**, 543–556.
- MICHALKE, A. 1965a On spatially growing disturbance in an inviscid shear layer. *J. Fluid Mech.* **23**, 521–544.
- MICHALKE, A. 1965b Vortex formation in a free boundary layer according to stability theory. *J. Fluid Mech.* **22**, 371–383.
- MONKEWITZ, P. A. 1974 Wake control. In *IUTAM Symposium: Bluff-Body Wakes, Dynamics and Instabilities*, pp. 227–240. Springer.
- MONKEWITZ, P. A. 1988 The absolute and convective nature of instability in two-dimensional wakes at low Reynolds numbers. *Phys. Fluids* **31**, 999–1006.
- MONKEWITZ, P. A., HUERRE, P. & CHOMAZ, J.-P. 1993 Global instability analysis of weakly non-parallel shear flows. *J. Fluid Mech.* **251**, 1–20.
- MONKEWITZ, P. A. & NGUYEN, L. N. 1987 Absolute instabilities in the near-wake of two-dimensional bluff bodies. *J. Fluids Struct.* **1**, 165–184.
- NISHIOKA, M. 1973 Hot-wire technique for measuring velocities at extremely low wind-speed. *Bull. JSME* **16**, 1887–1899.
- NORBERG, C. 1987 Effects of Reynolds number and a low-intensity freestream turbulence on the flow around a circular cylinder. PhD thesis, Chalmers Univ. Tech. Pub. No 87/2, S-412-96. Goteborg, Sweden.
- NORBERG, C. 1994 An experimental investigation of the flow around a circular cylinder: influence of aspect ratio. *J. Fluid Mech.* **258**, 287.
- PIER, B. 2002 On the frequency selection of finite-amplitude vortex shedding in the cylinder wake. *J. Fluid Mech.* **458**, 407–417.
- PIER, B. & HUERRE, P. 2001a Nonlinear self-sustained structures and fronts in spatially developing wake flows. *J. Fluid Mech.* **435**, 145–174.
- PIER, B. & HUERRE, P. 2001b Nonlinear synchronization in open flows. *J. Fluids Struct.* **15**, 471–480.
- PIER, B., HUERRE, P. & CHOMAZ, J.-M. 2001 Bifurcation to fully nonlinear synchronized structures in slowly varying media. *Physica D* **148**, 49–96.
- PIER, B., HUERRE, P., CHOMAZ, J.-M. & COUAIRO, A. 1998 Steep nonlinear global modes in spatially developing media. *Phys. Fluids* **10**, 2433–2435.
- PIERREHUMBERT, R. T. 1984 Local and global baroclinic instability of zonally varying flow. *J. Atmos. Sci.* **41**, 2141–2162.
- PRASAD, A. & WILLIAMSON, C. H. K. 1997 The instability of the shear layer separating from a bluff body. *J. Fluid Mech.* **333**, 375–402.
- PROVANSAL, M., MATHIS, C. & BOYER, L. 1987 Bénard–von Kármán instability: transient and forced regimes. *J. Fluid Mech.* **182**, 1–22.

- SATO, H. & KURIKI, K. 1961 The mechanism of transition in the wake of a thin flat plate placed parallel to a uniform flow. *J. Fluid Mech.* **11**, 321–352.
- SIPP, D. & LEBEDEV, A. 2007 Global stability of base and mean-flows: a general approach and its applications to cylinder and open cavity flows. *J. Fluid Mech.* **593**, 333–358.
- STRYKOWSKI, P. 1986 The control of absolutely and convectively unstable shear flows. PhD thesis, Yale University, New Haven, Connecticut, USA.
- THIRIA, B. & WESFREID, J. 2007 Stability properties of forced wakes. *J. Fluid Mech.* **579**, 137–161.
- THOMPSON, M. C. & HOURIGAN, K. 2005 The shear layer instability of a circular cylinder wake. *Phys. Fluids* **17**, 021702–5.
- THOMPSON, M. C., HOURIGAN, K. & SHERIDAN, J. 1996 Three-dimensional instabilities in the wake of a circular cylinder. *Expl Therm. Fluid Sci.* **12**, 190–196.
- TRIAANTAFYLLOU, G. S., TRIANTAFYLLOU, M. S. & CHRYSOSTOMIDIS, C. 1986 On the formation of vortex streets behind stationary cylinders. *J. Fluid Mech.* **170**, 461–477.
- UNAL, M. F. & ROCKWELL, D. 1988 On vortex formation from a cylinder. Part 1. The initial instability. *J. Fluid Mech.* **190**, 491–512.
- WEI, T. & SMITH, C. R. 1986 Secondary vortices in the wake of circular cylinders. *J. Fluid Mech.* **169**, 513.
- WILLIAMSON, C. & BROWN, G. 1998 A series in  $1/\sqrt{Re}$  to represent the Strouhal-Reynolds number relationship of the cylinder wake. *J. Fluids Struct.* **12**, 1073–1085.
- WILLIAMSON, C. H. K. 1989 Oblique and parallel modes of Vortex shedding in the wake of a circular cylinder at low Reynolds numbers. *J. Fluid Mech.* **206**, 579–627.
- ZDRAVKOVICH, M. 1997 *Flow around Circular Cylinders Volume 1: Fundamentals*, 1st edn. Oxford University Press.